MAP Decoding with Random Interleaver for MPEG-4 Image Indoor Wireless Transmission System

Srijidtra Mahapakulchai ‡ & Itsaree Sapasirisopon †
Department of Electrical Engineering, Kasetsart University, Bangkok, Thailand
‡ fengsjm@ku.ac.th, † itsaree_to@yahoo.com

***Abstract*—Here**, the investigation of the performance of MAP decoding with random interleaver for MPEG-4 image transmission system is described and analyzed. The performance evaluation is shown by setting MAP decoder to match the priori statistic of zerotree symbol sequence of the "Lena" image. In this work, we successfully reduce the computation of the random interleaver process by omitting the calculation of the interleaving matrix P. In some cases, despite the computational reduction, the slight improvement of about 0.5-1 dB in PSNR can still be obtained.

Keywords: MAP decoder, Random interleaver, Ring convolutional codes, Rician fading channels.

I. System Overview

The MPEG-4 source encoder produces the binary source-coded stream, which represents the coefficients of the lowest frequency subband (LFS) and higher frequency subbands (HFS). To increase the reliability of transmission, the binary sequence of HFS is divided into the variable length of packets. These binary sequence packets is transformed to symbol packets (2 bits/symbol) and then passed though our image transmission system as shown in Fig. 1. In the system,

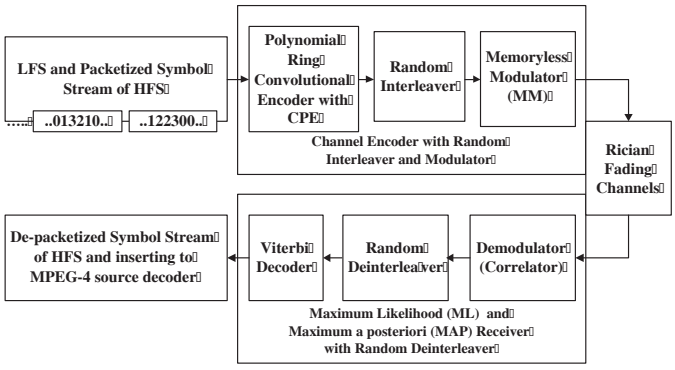

Fig. 1. System block diagram of the MPEG-4 still image transmission system using ring convolutional trellis codes with the random interleaver and deinterleaver.

we employ the channel encoder and modulator system, which are a rate $\frac{1}{2}$ polynomial convolutional encoder over ring of Z_4 (RCE) and CPFSK with $h = \frac{1}{4}$, respectively. The CPFSK system is decomposed into a continuous phase encoder (CPE) and a memoryless modulator (MM). The overall encoder is the combination of the RCE and the CPE. The coded symbol HFS packets from the overall encoder is then put into the variable size of random interleavers. This size is based upon the variable HFS packet length.

The MM maps a interleaved-coded symbol into the inphase and quadrature phase components of a baseband CPFSK signal. These two components are then corrupted by noise and distortion from Rician fading channel. At the receiver, we employ the maximum likelihood (ML) consisting of a demodulation process, the random deinterleaver, a branch metric calculator, and a Viterbi decoder. The decoded 4-ary stream is depacketized and fed into MPEG-4 source decoder resulting in a reconstructed image. Note that the performance of the system without the random interleaver/deinterleaver over Rician fading channel was recently summarized in our previous work [3].

II. MPEG-4 Image and Packet Structure

MPEG-4 embedded zerotree wavelet (EZW) is a version of the EZW algorithm proposed by the MPEG-4 committee in [4] and [5]. The encoding process begins with a transformation of an image by a discrete wavelet transform (DWT). In this case, we decompose an input image with a 5-level DWT using Daubechies (9,15) tap biorthogonal filters. Here, the wavelet coefficients of the lowest (coarsest) frequency subband (LFS) are coded separately from those of the higher (finer) frequency subbands (HFSs). This allows unequal error protection. Also, the number of spatial and signal-to-noise ratio (SNR) scalability levels is more flexible. The transformed coefficients in the LFS are encoded by a scalar quantizer followed by differential pulse code modulation (DPCM). The encoding of the wavelet coefficients in the HFS is done by successive approximation quantization process combined with the zerotree scanning.

In the MPEG-4 standard, the coding of the HFS can be categorized into two major modes, single quantization, and multi-quantization. In the single quantization mode, all wavelet coefficients are quantized only once with a multi-level quantizer. The bit allocation of the HFSs depends on the wavelet decomposition level. Note that the sequence of bits produced from this mode does not have the embedded code property, since the most significant bits of all wavelet coefficients are not transmitted first. Unlike the single quantization mode, the multi-quantization mode is the version of the original

EZW algorithm. In this mode, all wavelet coefficients are compared to a sequence of descending threshold values. When source coding with a high compression ratio such as EZW coding is employed, this coding becomes very sensitive to a noisy channel. In fact, a single bit error can lead to the destruction of the entire decoding process. This problem leads to a significant amount of research with the goal to increase the error resilience of source coding [6],[7] and [8]. The packet structures taken from [6] are reviewed. The basic structure of each packet illustrated in Figure 2 consists of compressed image bits; zerotree symbols and non-zero values, the cyclic redundancy check (CRC) and sufficient header information for independent packet decoding.

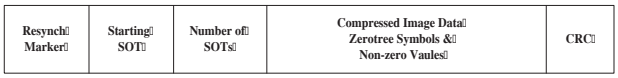

Fig. 2. The basic packet structure for the HFS.

The header contains twenty bits of resynchronization marker, ten bits of the location of the first spatial orientation tree (SOT) in an image, and eight bits for the number of the SOTs in a packet. Note that this configuration [6] is used for single quantization mode. For the multi-quantization mode, ten bits are required for the number of the SOTs. The cyclic redundancy check (CRC) is four bits long.

III. Polynomial Ring Convolutional Trellis Codes

For wireless channel application, we are interested in the modulation with the efficient bandwidth usage. The 4-ary continuous phase shift keying (4-ary CPFSK) with the modulation index h of 1/4 is the modulation of our choice. The signals of CPFSK occupy the bandwidth about the same as those of the minimum shift keying (MSK). As previously discussed, The decomposition of CPFSK system into CPE and MM allows us to algebraically combine CPE with the external RCE as the overall system channel encoder[10]. For instance, a rate 1/2 RCE is used in conjunction with a rate 1/2 CPE, and to be able to algebraically combine them into a single encoder, we need to first convert the CPE into an equivalent encoder of rate 2/4 [9] as shown in Eq.(1).

$$G_{CPE} = \begin{bmatrix} 1 & 0 & 3 & 1 \\ 3D & D & 1 & 0 \end{bmatrix}. \qquad (1)$$

We multiply the 32-state external RCE of rate 1/2 with the CPE of rate 2/4. We calculate the overall encoder as in Eq.(2).

$$\begin{aligned} G_{all}(D) &= \begin{bmatrix} 1+D+2D^3 \\ 2+D \end{bmatrix}^T \begin{bmatrix} 1 & 0 & 3 & 1 \\ 3D & D & 1 & 0 \end{bmatrix} \\ &= \begin{bmatrix} 1+3D+3D^2+2D^3 \\ 2D+D^2 \\ 1+2D^3 \\ 1+D+2D^3 \end{bmatrix}^T. \qquad (2) \end{aligned}$$

Notice that the multiplication of the rate 1/2 RCE with an equivalent CPE encoder of the 2/4 results in the overall encoder of rate 1/4. It is worth mentioning that the MM maps the 4 output symbols of the rate 2/4 of CPE into only two CPFSK signals. In another word, a CPFSK signal is obtained from 2 output symbols;one for the beginning of the phase and another one for the phase transition.

When the feedback-free form of convolutional encoder is applied, one must concern whether or not the code is catastrophic. It means that the codeword of finite errors can lead to the decoded information bit of an infinite error. In order to avoid using a catastrophic encoder, we perform the noncatastrophic encoder check. Detail about the theorems and algorithms can be found in [11].

IV. Random Interleavers

Like any interleaving process, random interleaving process can be used to alleviate the lost of data from bursty noise. There are many works which evaluate the performance of random interleavers such as [12] and [13]. S. Benedetto and his colleague [12] consider the analysis and design of serial concatenation of interleaved codes. L.Dinoi and S. Benedetto [13] propose the algorithm of designing good semi-random interleavers for both parallel and serially concatenated codes. In this work, we emphasize the use of random interleavers for the variable length of HFS packets, L. The interleaving process is done after passing each packet through the rate $\frac{1}{2}$ channel encoder. Therefore, the interleaving range is twice of the length of each packet. We compute the interleaved data as $\mathbf{d_{INT}} = \mathbf{dP}$, where $\mathbf{d}$ is a data vector and P is a random matrix. Note that in our case, the size of a data vector $\mathbf{d}$ is twice of the packet length, $2L = L_T$. Moreover, to generate the matrix P, we begin with the $L_T \times L_T$ identity matrix. Then we reorder each row randomly. The random algorithm is based upon linear congruence method [14]. The algorithm generates the $m \times m$ interleaving matrix P, from the permutated random sequence $\mathbf{x} = \{x_n\}_{n=0}^{m-1}$, whose elements are computed by recursive substitution of the equation:

$$x_{n+1} = (ax_n + c) \bmod m, \quad n = 0, 1, \ldots, m, \qquad (3)$$

where $x_n \in \{0, 1, \ldots, m-1\}$; x_0 can be any integer in the set $\{0, 1, \ldots, m-1\}$; a and c are constant chosen by the following procedure:

- Step 1: Let b_0 be the product of all non-repeated prime factors of m.
- Step 2: Set $b = vb_0$, where v is a prime number such that $b = vb_0 \leq m$.
- Step 3: Compute $a = b + 1$.
- Step 4: Choose c such that c and m are relatively prime and $1 < c < m$.

Once the permutated random sequence $\mathbf{x} = \{x_n\}_{n=0}^{m-1}$ is generated by recursively substituting x_n in Eq.(3) for $n = 0, 1, \ldots, m-1$. The corresponding interleaving matrix P can be generated by reordering the rows of $m \times m$ identity matrix according to the random sequence $\mathbf{x}$.

Example: For $m = 10$, one can generate a random interleaving matrix as follows:

First, compute $b_0 = (2)(5) = 10$ since prime factorization of m is $m = (2)(5)$. Next, $b = vb_0 = (1)(10) = 10$, by choosing $v = 1$. So, $a = b+1 = 11$. For $m = 10, c$ can possibly be 3 or 7 since c and m must be relatively prime and $1 < c < 10$. If one let $c = 7$ and $x_0 = 1$, and recursively substitute $n = 0, 1, \ldots, 9$ in Eq.(3), one obtains $\mathbf{x} = \{1, 8, 5, 2, 9, 6, 3, 0, 7, 4\}$. Note that the number in sequence $\mathbf{x}$ are associated with the location of 1 in each columns of matrix P.

Note that the generation of the matrix P is not unique and depends on the choices of v, c, and x_0, which can be chosen randomly to generate many random matrices P. Furthermore, by simple verification, one can show that the resulting matrix P is unitary i.e. $PP^T = P^T P = I$ or $P^{-1} = P^T$, where $(\cdot)^T$ is the transpose operation and I is the identity matrix. This is particularly important since P^{-1} is corresponding to the deinterleaving operation and can be easily computed by transpose operation rather than the more complicated procedure of inverse matrix computation. For the deinterleaving process, we obtain a data vector by calculating $\mathbf{d}$ as $\mathbf{d} = \mathbf{d}_{INT} P^T$.

To reduce the computation of interleaving process, we do not generate the matrix P. Instead, we find the location of deinterleaved data by searching for the location of number $0, 1, \ldots, m-1$ in the random sequence $\mathbf{x}$ respectively. For the above example, the location of number 0 in random sequence $\mathbf{x} = \{1, 8, 5, 2, 9, 6, 3, 0, 7, 4\}$. is 7. The location of number 1 is 0 and so on. Finally we obtain the deinterleaved data vector by reordering the interleaved data vector associated with sequence $\{7, 0, 3, 6, 9, 2, 5, 8, 1, 4\}$.

V. Rician Fading Channel

It is commonly known that the Rayleigh and Rician statistics are suitable for modelling an indoor wireless channel [17], [18]. This channel is suffer from the multiple reflections from both indoor building walls and objects inside. In this paper, we focus on the performance of the system over a slow-flat Rician fading channel.

Let the transmitted baseband signal is $s_l(t)$. The received equivalent lowpass signal can be written as

$$r_l(t) = (1 + \beta e^{-j\phi}) s_l(t) + n_{wl}(t), 0 \le t \le T, \quad (4)$$

where n_{wl} is the complex-valued white Gaussian noise random process with two-sided spectral density $N_0/2$. Since the channel is sufficiently slow, the phase shift ϕ can be estimated from the received signal. Without loss of generality, we assume ϕ to be zero. The parameter β is defined as

$$\beta = \sqrt{(f_i(t)/\sqrt{2S})^2 + (f_q(t)/\sqrt{2S})^2}, \quad (5)$$

where $f_i(t)$ and $f_q(t)$ are the in-phase and quadrature phase components of the scattered multipath signal, which are Gaussian random variables with zero mean and variance equal to σ^2. S is the signal power, $S = Es/T$, where T is a symbol interval. Let γ_b be $(1+\beta)^2 E_s/N_0$. The probability density function of γ_b can be found in [19] as

$$p(\gamma_b) = \frac{1+\gamma}{\bar{\gamma_b}} e^{-\gamma-(1+\gamma)\gamma_b/\bar{\gamma_b}} I_0\left(2\sqrt{\frac{\gamma(1+\gamma)\gamma_b}{\bar{\gamma_b}}}\right), \quad (6)$$

where

$$\bar{\gamma_b} = \frac{1+\gamma}{\gamma} E_s/N_0, \quad (7)$$

and $\gamma = S/\sigma^2$ is the ratio of the direct path power to the scattered path power. If the direct path is blocked by any structures, the fading channel is called a Rayleigh channel. The channel can be simulated by letting the signal power S be small compared to the scattered path power σ^2.

VI. MAP Decoding Derivation for Rician Fading Channels

To construct the MAP decoder for the CPFSK system, we observe the data samples $z_{k,i}$. During time interval $kT \le t \le (k+1)T$, the observed samples can be written as $z_{k,i} = (1+\beta)s_{m,k,i} + n_{k,i}$ where $i = 1, 2, \cdot, N$. For a slowly fading channel, β is a constant during each signal interval. Al Semari *et al.* [15] assume that the fading values can de determined, *i.e.* they estimate channel state information (CSI). Therefore, this information can be incorporated into the decoding metric. We first follow this assumption. However, we shall show later that by using only the mean value of β, no estimation is necessary, and some improvement is still obtained. Assuming CSI, the conditional probability becomes

$$P(z_k|s_{m,k}) = \frac{1}{(\sqrt{\pi N_0})^N} e^{-\left[\sum_{i=1}^{N} \frac{(z_{k,i}-\alpha s_{m,k,i})^2}{N_0}\right]}, \quad (8)$$

where $\alpha = (1+\beta)$. The designed MAP decoding is based on a kind of probabilistic decoder known as Viterbi decoder [16]. This decoder is said to be "optimal" because it is the solution to the problem of maximum *a posteriori* probability (MAP) estimation of the state sequence of a finite-state discrete-time Markov process. This estimation problem is equivalent to finding the state sequence for $P(\mathbf{z}|\mathbf{x})P(\mathbf{x})$ is maximum, where $\mathbf{z}$ and $\mathbf{x}$ are the observed and state sequences respectively. By considering the first order Markov process and memoryless noise properties, we aim to search for the state sequence $\mathbf{x}$ which satisfies arg $\max_{\mathbf{x}} P(\mathbf{z}|\mathbf{x})P(\mathbf{x})$. And it is equal to

$$\arg \max_{\mathbf{x}} \prod_{k=0}^{K-1} P(z_k|x_k, x_{k-1}) P(x_k|x_{k-1}). \quad (9)$$

Since the natural log function, ln(.) is a monotonic function, we can apply this function to Eq.(9) without changing its solution. Also, we define the negative value of the component inside the summation as the branch metric, $\lambda(x_k, x_{k-1}) = -\ln P(z_k|x_k, x_{k-1}) - \ln P(x_k|x_{k-1})$. we obtain the branch metric $\lambda(s_{m,k})$ as $\lambda(s_{m,k}) = -\sum_{i=1}^{N} z_{k,i}s_{m,k,i} - \frac{N_0}{2\alpha}\ln P(x_{2,k+1}|x_{2,k})$. Since $P(x_{2,k+1}|x_{2,k}) = P(u_k|u_{k-1}) = P(u_{k+1}|u_k)$, where $\mathbf{u}$ is the input sequence. The new branch metric becomes $-\sum_{i=1}^{N} z_{k,i}s_{m,k,i} - \frac{N_0}{2\alpha}\ln P(u_k|u_{k-1})$. When an external encoder (CE) is included in the system, we have to consider the conditional probability $P(z_k|S_{0,k+1}, S_{0,k})$. The difference here is that the effect of the fading amplitude is included in the computation of the conditional probability $P(z_k|S_{0,k+1}, S_{0,k})$ via the relationship in Eq. (8). Therefore the branch metric becomes

$$\lambda(s_{m,k}) = -\alpha_1 \sum_{i=1}^{N} z_{k,i}s_{m,k,i} - \alpha_2 \sum_{i=N+1}^{2N} z_{k,i}s_{m,k,i} - \frac{N_0}{2}\ln P(S_{0,k+1}|S_{0,k}), \quad (10)$$

where α_1 and α_2 are the constant fading amplitude during the first and second signal interval, respectively.

VII. Simulation Results

The famous "Lena" image is chosen as our tested information source. This raw-pgm grayscale image has a size of 512×512 pixels. The image is compressed by applying the EZW algorithm. In this work, five decomposition levels are implemented, resulting in 16 subbands; one subband is for the lowest frequency subband (LFS) and the rest is the higher frequency subbands (HFS(s)). The wavelet coefficients of all HFS(s) are quantized into the bit stream and then divided into variable length of packets. For this particular image, we obtain the number of HFS packets of 101 with the nominal packet length of about 325 symbols. For a noiseless channel, the peak signal to noise ratio (PSNR) of the reconstructed image and its compression ratio is 31.83 dB and 31:1, respectively.

For the system channel encoder, we select the 32-state polynomial ring convolutional encoder from our previous work [2]. Turning to interleaving process, we implement the variable length of random interleavers which corresponds to the variable length of 101 HFS packets.

Table I, II and Table III summarize the average word error rates (WER) and peak signal to noise ratio (PSNR) for the Rician channels with $\gamma = -43$ dB, -33 dB and -23 dB, respectively. Note that when $\gamma = -\infty$ dB, the Rician statistic approaches Rayleigh. The simulations are done by using 300 lena images within the interest range of $\bar{\gamma_b} = 3.75, 5.00$, and 6.25 dB. The second column of all Tables shows the results when the random interleavers are applied for all HFS packets but not LFS. And the last column shows the results when LFS and all HFS packets are interleaved.

TABLE I

The average PSNR of the reconstructed "Lena" image using ML and MAP decoding for Rician channel with $\gamma = -43$ *dB*.

$\overline{\gamma_b}$ (dB)	PSNR (dB) with interleavers except LFS (WER)		PSNR (dB) with interleavers (WER)	
	ML decoding	MAP decoding	ML decoding	MAP decoding
3.75	20.63 (0.0022)	20.51 (0.0026)	20.52 (0.0022)	20.39 (0.0026)
5.00	25.49 (0.00065)	25.41 (0.00073)	25.82 (0.00065)	25.74 (0.00073)
6.25	28.96 (0.00022)	28.87 (0.00025)	28.75 (0.00022)	28.67 (0.00025)

TABLE II

The average PSNR of the reconstructed "Lena" image using ML and MAP decoding for Rician channel with $\gamma = -33$ *dB*.

$\overline{\gamma_b}$ (dB)	PSNR (dB) with interleavers except LFS (WER)		PSNR (dB) with interleavers (WER)	
	ML decoding	MAP decoding	ML decoding	MAP decoding
3.75	21.82 (0.0017)	21.61 (0.002)	21.73 (0.0017)	21.50 (0.002)
5.00	26.53 (0.0005)	26.38 (0.00058)	26.72 (0.00049)	25.58 (0.00058)
6.25	29.45 (0.00017)	29.34 (0.0002)	29.29 (0.00017)	29.19 (0.0002)

We can observe that for all cases, the average PSNRs (dB) for MAP decoding are slightly lower than those for ML decoding. This may be because the mismatch on priori probability of zerotree symbol after interleaving process. It is mentioned that MAP decoding is employed only zerotree symbols while ML decoding is used for the rest. Moreover, we notice that the effect of interleavers is on the location of symbol errors, not in the number of symbol errors. Of course, when there is the change in the location of symbol errors, the PSNR of the reconstructed image will be changed.

Fig. 3 (A) and (B) are the reconstructed images in which result from the simulation at $\bar{\gamma_b}$ of 5 dB and γ of -33 dB, respectively. This is the case when the interleavers are in great help. The slight improvement (about 1 dB) is visually noticeable on area in the lower left corner of the image. We also obtain the additional clearness on the Lena's sun-hat and shoulder areas.

VIII. Conclusion and Future Work

The system performances with the variable-size random interleavers for Rician fading channel are summarized. The system channel encoder is the combination of convolutional encoder over ring Z_4 and CPFSK modulation. At the receiver, the conventional ML and MAP Viterbi decoder are employed. The results in some noise patterns show the slight improvement in PSNRs, while some do not.

TABLE III

The average PSNR of the reconstructed "Lena" image using ML and MAP decoding for Rician channel with $\gamma = -23$ *dB*.

$\overline{\gamma_b}$ (dB)	PSNR (dB) with interleavers except LFS (WER)		PSNR (dB) with interleavers (WER)	
	ML decoding	MAP decoding	ML decoding	MAP decoding
3.75	25.04 (0.00079)	24.88 (0.0009)	25.39 (0.00078)	25.24 (0.0009)
5.00	28.76 (0.00024)	28.60 (0.00028)	28.65 (0.00023)	28.49 (0.00027)
6.25	30.56 (0.00008)	30.47 (0.0001)	30.47 (0.00009)	30.39 (0.0001)

For future work, we will focus on the range of $\overline{\gamma_b}$ which is corresponded to PSNRs of about 25-26 dB. We attempt to improve PSNRs at these ranges by applying semi-random interleaver (S-random).

IX. Acknowledgement

This research work is financially supported by the Kasetsart University Research and Development Institute (KURDI) under the research project grant of fiscal year 2007-2008. Moreover, the authors would like to thank for all reviewer's comments.

Fig. 3. $\boxed{\frac{(A)}{(B)}}$ Reconstructed "Lena" image using random interleaver. (A) The $\overline{\gamma_b} = 5$ dB with ML decoding. PSNR =27.28 dB. WER = 0.00038. (B) The $\overline{\gamma_b} = 5$ dB with MAP decoding. PSNR = 28.51 dB. WER = 0.00032.

References

[1] S. Mahapakulchai and R. E. Van Dyck, "Design of ring convolutional trellis codes for MAP decoding of MPEG-4 imagery," *Proc. IEEE Inter. Conf. Comm. (ICC 2001)*, June 2001.

[2] S. Mahapakulchai and R. E. Van Dyck, "Design of ring convolutional trellis codes for MAP decoding of MPEG-4 images," *IEEE Trans. Comm.*, July 2004.

[3] S. Mahapakulchai, "MAP decoding for polynomial ring convolutional trellis codes for MPEG-4 image transmission system over Rician fading channel, " *Proceeding of the 2007 Electrical Engineering/Electronic, Computer, Telecommunications and Information Technology (ECTI) International Conference*, vol. 2, pp. 655-658, May 2007.

[4] ISO/IEC JTC1/SC29/WG11, "Information technology, coding of audio-visual objects: Visual, ISO/IEC 14496-2, Committee Draft," *N2202*, Mar. 1998.

[5] ISO/IEC JTC1/SC29/WG11, "MPEG-4 video verification model version 11.0," *N2172*, Mar. 1998.

[6] R. E. Van Dyck, "MPEG-4 image transmission using MAP source-controlled channel decoding," *IEEE JSAC*, vol. 18, pp. 1087-1098, June, 2000.

[7] P. G. Sherwood and K. Zeger, "Progressive Image Coding for Noisy Channels," *IEEE Signal Processing Letter*, vol. 4, no. 7, pp. 189-191, Jul. 1997.

[8] H. Man, F. Kossentini, and M. J. T. Smith, "Robust EZW image coding for noisy channels," *IEEE Signal Proc. Letters*, vol. 4, no. 8, pp. 227-229, Aug. 1997.

[9] R. H. Yang, and D. P. Taylor, "Trellis-coded continuous-phase frequency-shift keying with ring convolutional codes, " *IEEE Trans. Information Theory*, vol. 40, pp. 1057-1067, Jul. 1994.

[10] B. E. Rimoldi, "A decomposition approach to CPM, " *IEEE Trans. Info. Theory*, vol. 34, no. 2, pp. 260-270, Mar. 1988.

[11] G. David Forney, Jr, "Convolutional codes I: Algebraic structure," *IEEE Trans. Inform. Theory*, vol. IT-16, no. 6, pp. 720-738, Nov. 1970.

[12] S. Bennedetto, D. Divsalar, G. Montorsi and F. Pollara," Serial concatenation of interleaved codes: Performance analysis, design, and iterative decoding," *IEEE Trans. Inform. Theory*, vol. 44, no. 3, pp. 909-926, May 1998.

[13] L. Dinoi and S. Benedetto," Variable-size interleaver design for parallel Turbo decoder architectures," *IEEE Trans. Commu.*, vol. 53, no. 11, pp. 1833-1840, Nov. 2005.

[14] D. M. Burton, *Elementary number theory*, McGraw Hill, 2007.

[15] S. A. Al-Semari, F. Alajaji, and T. Fuja, "Sequence MAP decoding of trellis codes for Gaussian and Rayleigh Channels," *IEEE Trans. on Vehicular Tech.*, vol. 48, pp. 1130-1140, July 1999.

[16] G. D. Forney, Jr, "The Viterbi algorithm," *Proc. of the IEEE*, vol. 61, pp. 268-278, Mar. 1973.

[17] R. Ganesh and K. Pahlavan, "On the modeling of fading multipath indoor radio channels," *Proc. IEEE ICC'89*, pp. 1346-1350, June 1989.

[18] A. M. Saleh and R. A. Valenzuela, "A statisticall model for indoor multipath propagation," *IEEE J. Select. Areas Commun.*, vol. SAC-5, pp. 128-137, Feb. 1987.

[19] H. M. Kwon, "Performance of continuous-phase frequency shift keying under fading," *IEEE Global Comm. Conf. (GLOBECOM'94)* vol. 3, pp. 1358-1362, November 1994.